

Feasibility of apparent diffusion coefficient in predicting the technical outcome of MR-guided high-intensity focused ultrasound treatment of uterine fibroids – a comparison with the Funaki classification

Teija Sainio , Jani Saunavaara , Gaber Komar , Sami Mattila , Saara Otonkoski , Kirsi Joronen , Antti Perheentupa & Roberto Blanco Sequeiros

To cite this article: Teija Sainio , Jani Saunavaara , Gaber Komar , Sami Mattila , Saara Otonkoski , Kirsi Joronen , Antti Perheentupa & Roberto Blanco Sequeiros (2021) Feasibility of apparent diffusion coefficient in predicting the technical outcome of MR-guided high-intensity focused ultrasound treatment of uterine fibroids – a comparison with the Funaki classification, International Journal of Hyperthermia, 38:1, 85-94, DOI: [10.1080/02656736.2021.1874545](https://doi.org/10.1080/02656736.2021.1874545)

To link to this article: <https://doi.org/10.1080/02656736.2021.1874545>



© 2021 The Author(s). Published with license by Taylor & Francis Group, LLC



Published online: 28 Jan 2021.



Submit your article to this journal [↗](#)



Article views: 271









View related articles [↗](#)



View Crossmark data [↗](#)

Feasibility of apparent diffusion coefficient in predicting the technical outcome of MR-guided high-intensity focused ultrasound treatment of uterine fibroids – a comparison with the Funaki classification

Teija Sainio^a , Jani Saunavaara^a , Gaber Komar^b , Sami Mattila^a, Saara Otonkoski^c, Kirsi Joronen^c , Antti Perheentupa^c  and Roberto Blanco Sequeiros^b 

^aDepartment of Medical Physics, Turku University Hospital, Turku, Finland; ^bDepartment of Radiology, Turku University Hospital, Turku, Finland; ^cDepartment of Obstetrics and Gynecology, Turku University Hospital, Turku, Finland

ABSTRACT

Purpose: To investigate the feasibility of using an apparent diffusion coefficient (ADC) classification in predicting the technical outcome of magnetic resonance imaging-guided high-intensity focused ultrasound (MRgHIFU) treatment of symptomatic uterine fibroids and to compare it to the Funaki classification.

Materials and methods: Forty-two patients with forty-eight uterine fibroids underwent diffusion-weighted imaging (DWI) before MRgHIFU treatment. The DW images were acquired with five different b-values. Correlations between ADC values and treatment parameters were assessed. Optimal ADC cut-off values were determined to predict technical outcomes, that is, nonperfused volume ratios (NPVr) such that three classification groups were created (NPVr of <30%, 30–80%, or >80%). Results were compared to the Funaki classification using receiver-operating-characteristic (ROC) curve analysis, with statistical significance being tested with the Chi-square test.

Results: A statistically significant negative correlation (Spearman's $\rho = -0.31$, p -value < 0.05) was detected between ADC values and NPV ratios. ROC curve analysis indicated that optimal ADC cutoff values of $980 \times 10^{-6} \text{mm}^2/\text{s}$ (NPVr > 80%) and $1800 \times 10^{-6} \text{mm}^2/\text{s}$ (NPVr < 30%) made it possible to classify fibroids into three groups: ADC I (NPVr > 80%), ADC II (NPVr 30–80%) and ADC III (NPVr < 30%). Analysis of the whole model area under the curve resulted in values of 0.79 for the ADC classification (p -value = 0.0007) and 0.62 for the Funaki classification (p -value = 0.0527).

Conclusions: Lower ADC values prior to treatment correlate with higher NPV ratios. The ADC classification seems to be able to predict the NPV ratio and may even outperform the Funaki classification. Based on these results DWI and ADC maps should be included in the MRI screening protocol.

ARTICLE HISTORY

Received 16 March 2020
Revised 18 December 2020
Accepted 6 January 2021

KEYWORDS

Uterine fibroid; high intensity focused ultrasound; diffusion-weighted imaging; thermal ablation; MRI

1. Introduction

Magnetic resonance-guided high-intensity focused ultrasound (MRgHIFU) ablation therapy has been demonstrated to be a safe and effective non-invasive treatment for symptomatic uterine fibroids [1–4]. Immediately after the treatment ablated tissue can be assessed from T1-weighted contrast-enhanced images as non-enhancing regions also known as the nonperfused volume (NPV) which can be used to calculate the nonperfused volume ratio (NPVr), that is, nonperfused fibroid volume/total fibroid volume. A higher NPVr value, that is, technical outcome, has been shown to correlate with a positive clinical treatment outcome [5,6]. However, due to differences in tissue densities and vascularity, not all fibroids are suitable for MRgHIFU therapy [2–4]. Therefore, uterine fibroid characterization prior to the MRgHIFU treatment is usually performed with different techniques. Histopathologically poor MRgHIFU treatment outcomes are often associated with high cellularity and

increased vascularity of uterine fibroid [7–9]. On the other hand, several MRI-related factors have been shown to predict the technical treatment outcome (i.e., NPVr) or treatment efficiency parameters (i.e., heating and ablation efficiencies), for example, the T2-weighted signal intensity (Funaki classification) [10], fibroid perfusion parameters [11–14], and texture parameters [15]. The Funaki classification is based on T2 weighted images in which the signal intensity of fibroid is compared to myometrium and muscle signal intensities: hypointense (Funaki I), intermediate (Funaki II), and hyperintense (Funaki III). Even though the Funaki classification is widely used in predicting the outcome of uterine fibroid therapy, it only provides a qualitative assessment of the suitability of a fibroid for HIFU therapy. On the other hand, quantitative methods could be more reliable in predicting the technical outcome. While dynamic contrast-enhanced MRI can provide quantitative information about perfusion, it also requires extensive expertise in image acquisition and

post-processing and is therefore not routinely used in clinical practice.

Diffusion-weighted imaging (DWI) is a widely exploited MR imaging technique that can provide quantitative information on tissue structures and processes, such as cellularity and microcirculation [16–20]. The technique is based on acquiring images with several different diffusion weightings, that is, b-values, utilizing diffusion encoding gradients. From these images, apparent diffusion coefficient (ADC) maps can be calculated. ADC values in biological tissues reflect the motion of water molecules in different compartments: intracellular, extracellular, and the intravascular space (perfusion). This leads to a non-mono-exponential behavior of the signal intensity decay as a function of the b-value. ADC maps obtained from low b-value images (0–200 s/mm²), are believed to reflect the perfusion effects [17,18,21–23].

The choice of b-values used for ADC calculation has been shown to influence the ADC value measured in uterine fibroid tissue, which indicated that DWI in fibroids reflects both diffusion and perfusion effects [23]. Previous investigators have also reported that DWI can be used to evaluate ablated tissue during MRgHIFU treatment of uterine fibroids [23–25]. As far as we are aware, no reports have been published about the potential usefulness of ADC values to predict whether uterine fibroids are good candidates for MRgHIFU therapy prior to the treatment. Previous studies have revealed that b-values of 0, 100, 400, 600 and 800 s/mm² could detect both perfusion and diffusion effects in uterine fibroids and therefore, same the b-values were used in this study [23–25].

The aim of this study was to evaluate the correlation between ADC values and NPV ratios and to assess the feasibility of the ADC classification in predicting the technical outcome of magnetic resonance-guided high-intensity focused ultrasound treatment of symptomatic uterine fibroids and to compare it to the Funaki classification.

2. Materials and methods

2.1. Patients

This study was approved by the Ethics Committee of the Hospital District (ETMK: 95/1801/2015 16.6.2015). Written informed consent for the MRgHIFU procedure was obtained from all patients.

A total of 64 patients were enrolled for the MRgHIFU treatment of uterine fibroids between May 2016 and December 2018. Inclusion criteria for the MRgHIFU treatment were symptoms caused by fibroids, physical and mental health appropriate for an MRI scan, uterine fibroid diameter 2.5–10 cm, and premenopausal status. Exclusion criteria for the MRgHIFU treatment were major uterine anomalies, major scarring of the lower abdomen, degenerated fibroid, and suspicion of malignancy. The enrolled patients for this study had to meet the following inclusion criteria: (1) oxytocin was not used during MRgHIFU treatment, (2) patient had undergone diffusion-weighted imaging before MRgHIFU treatment, (3) there were no significant artifacts on the ADC map in order to reliably measure the mean ADC value from the

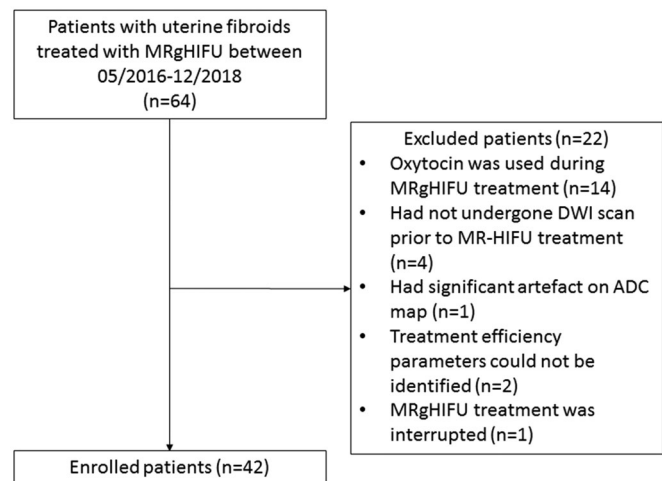


Figure 1. A CONSORT flow diagram of patient selection process in this study.

uterine fibroid, (4) treatment efficiency parameters could be identified for each treated fibroid, and (5) MRgHIFU treatment had not been interrupted. A total of 42 patients were enrolled for this study, and 22 patients were excluded from the analysis due to the following reasons: oxytocin had been used during MRgHIFU treatment (14 patients), DWI scan had not been performed prior to MRgHIFU treatment (4 patients), a large artifact on ADC map from the air inside the rectum (1 patient), treatment parameters could not be identified for each fibroid due to a cumulative heating effect (2 patients), and interrupted treatment due to the patient experiencing significant discomfort during sonications (1 patient), see CONSORT diagram (Figure 1).

2.2. Screening MRI

Twenty-five patients had screening MRI performed with the same MRI scanner (Ingenia 3.0T, Philips Healthcare, Best, The Netherlands) which has an integrated MRgHIFU system (Sonalleve V2, Profound Medical Inc., Mississauga, Canada) and seventeen patients had their screening MRI performed in their local hospital with different MRI scanners. The screening MRI protocol in our hospital involved T2-weighted, T1-weighted, diffusion-weighted and contrast-enhanced T1-weighted imaging (Table 1). The screening MRI protocol in other hospitals usually included T2-weighted, T1-weighted and contrast-enhanced T1-weighted imaging with slightly varying sequence parameters. Sagittal T2-weighted images were used for the determination of the Funaki classification: mean echo time 97 ms (range: 75–128 ms) and mean repetition time 4973 ms (range: 3510–10,412 ms). From these images, the interventional radiologist (GK) evaluated the number, size, T2 signal intensity, that is, the Funaki classification, enhancement in T1-weighted images and the depth of uterine fibroid(s), the presence of abdominal scars, the position of bowel loops, and the thickness of the subcutaneous fat layer of the abdominal wall.

The T2 signal intensity (SI) of uterine fibroid(s), abdominal muscle, and myometrium were obtained from regions of interest (ROIs) and relative T2 signal intensities (rT2) were calculated (average SI of fibroid/average SI of skeletal muscle

Table 1. MR imaging parameters.

Parameter	T2W TSE	T2W TSE	T1W TFE	DWI	CE-T1W TFE	MR thermometry FFE-EPI
Imaging plane	Sagittal	Axial	Sagittal	Axial	Sagittal	Coronal/Sagittal
Repetition time (ms)	4844	3845	5.2	3733	5.2	37
Echo time (ms)	95	80	2.6	83	2.6	19.5
Flip angle (°)	90	90	7	90	7	19
Number of slices	42	45	133	30	133	6
Section thickness (mm)	3	4	3	5	3	7
Matrix size (mm)	344 × 267	272 × 241	172 × 298	124 × 96	172 × 298	192 × 143
Field of view (mm)	240 × 240	300 × 300	255 × 448	375 × 290	255 × 448	400 × 300

CE: contrast-enhanced; DWI: diffusion-weighted imaging; EPI: echo planar imaging; FFE: fast field echo; TFE: turbo field echo; TSE: turbo spin echo.

and average SI of fibroid/average SI of myometrium). The ROIs were drawn with Osirix software (v.7.0, Pixmeo) on sagittal T2-weighted images on fibroid, myometrium, and abdominal muscle. From these signal intensities, the Funaki classification was determined: Funaki I, hypointense (comparable to that of skeletal muscle); Funaki II, intermediate (lower than that of the myometrium but higher than that of the skeletal muscle); and Funaki III, hyperintense (equal to or higher than that of the myometrium).

2.3. Diffusion-weighted imaging

Diffusion-weighted imaging was performed during screening MRI using a torso coil with 32 channels (8 patients) or prior MRgHIFU treatment with a HIFU coil system which consists of two coils with a total of 5 channels (34 patients).

In order to avoid breathing artifacts and susceptibility artifacts of metal objects (HIFU transducer and coil element on the treatment window), two saturation slabs were used in the DWI scan and they were placed on the abdominal and dorsal fat. The DW images were acquired with b-values of 0, 100, 400, 600 and 800 s/mm². The ADC maps were reconstructed from the DW images for quantitative analysis with different combinations of b-values: (1) all b-values, (2) the lowest two b-values to emphasize the perfusion effects (0 and 100 s/mm²), and the highest b-values to capture the diffusion effects (400, 600 and 800 s/mm²), using the MRI scanner software (Philips).

ROIs were drawn with Osirix software (v.7.0, Pixmeo) in the three middle slices of the fibroid to include most of the fibroid while avoiding the partial volume effect of large 5 mm voxels caused by tissue borders. This was achieved by placing the ROI border a few millimeters inside the fibroid. The ROI size was therefore dependent on the size of the fibroid. The ROIs were then copied to all ADC maps in the same three sequential slices, and averaged quantitative ADC values were obtained from each ADC map.

2.4. MRgHIFU system and treatment procedure

All treatment procedures were performed using an extracorporeal, clinical tabletop MRgHIFU system (Sonalleve V2, Profound Medical Inc., Mississauga, Canada) equipped with a direct skin cooling device in combination with a 3.0T clinical MR scanner (Ingenia, Philips, Best, the Netherlands).

The patient preparation, procedure and medication were performed as previously described [19]. The radiologist (GK) planned the treatment by positioning the ellipsoid treatment

cells (axial diameters: 4, 8, 12, 14 and 16 mm) into the targeted fibroid one by one exploiting the one-layer strategy [12]. The cell size was chosen to be as large as possible with respect to the fibroid volume. Therapy sonication was determined using low power (50–70 W) test sonication. The available therapy sonication power range was 140–300 W. The optimal cell type was chosen so that as large an ablation as possible could be achieved by one sonication. The sonication time was determined by the cell type. A regular cell had a predetermined sonication time and the feedback cell stopped the sonication when thermal dose-volume achieved the cell volume or when maximum time is reached. During the sonication, heating of the targeted area and possible undesired heating of surrounding tissue were monitored with real-time MR thermometry by using the proton resonance frequency shift technique (Table 1) in six slices (near field: one coronal slice, target: three coronal slices and one sagittal slice, and far-field: one coronal slice). The temperature maps were overlaid on the magnitude images which enabled monitoring of the anatomy and movement during the sonications. From the temperature maps, thermal dose maps were calculated by the system according to the Sapareto–Dewey equation (in units of cumulative equivalent minutes at 43 °C [CEM43]) [20]. The contour lines of the area of a lethal thermal dose (i.e., ≥240 CEM43) were automatically displayed by the system on each thermal map slice. From the 240 CEM43 contour lines the system automatically estimated the lethal thermal dose-volume [21].

Immediately after the treatment, contrast-enhanced T1-weighted images were acquired by injecting the contrast agent (DOTAREM, Guerbet, Aulnay-Sous-Bois, France, 0.1 mmol/kg) to evaluate the NPV.

2.5. Treatment outcome and efficiency parameters

The NPV and uterine fibroid volumes were computed from T1-weighted CE and T2-weighted images, respectively, using manual segmentation on the image analysis software (AW-server 3.2, GE Healthcare). Finally, the NPVr recognized as a good predictor of HIFU clinical outcome was calculated as the NPV/fibroid volume [5,6].

Both heating and ablation efficiencies of MRgHIFU were investigated for each fibroid. Heating efficiency was defined as the total volume of 240 CEM43 contours divided by the total volume of treatment cells (%), and ablation efficiency was defined as the nonperfused volume divided by the total volume of treatment cells (%), similarly as in previous studies [13,15,22]. Available treatment cell sizes were 4, 8, 12, 14 and

16 mm, corresponding to estimated ablation volumes of 0.08, 0.67, 2.26, 3.59 and 5.36 mL, respectively. Prematurely terminated sonications (<10 s) were excluded from the calculations in order to avoid an overestimation of the total treatment cell volume [23]. The overlap between treatment cells was considered negligible.

Another way to define heating efficiency could be to utilize the total volume of 240 CEM43 contours divided by the total delivered acoustic energy at the focus (mL/J) per treatment. When calculated this way, heating efficiency is not dependent on the cell type, the therapy power used, or the patient's anatomy. In order to determine the total delivered acoustic energy at the focus, and attenuation correction was estimated by determining the ultrasound attenuation for each layer: HIFU system oil bath, HIFU system direct skin cooling device (water), gel pad, subcutaneous fat layer, the muscle layer, visceral fat layer, bladder layer (urine) and fibroid. Each layer thickness was measured from five different pathways of the ultrasound beam: center, superior, inferior, right and left, until focus was reached by using treatment planning 3D T2-weighted images. Each layer thickness was averaged for calculating the total attenuation:

$$a_{total}(dB) = \sum_i a_i \cdot \bar{d}_i \cdot f \quad (1)$$

where a_i is the attenuation coefficient [dB/m/MHz] of the medium (i), \bar{d}_i is the averaged layer thickness of the medium (i) and f is the used ultrasound frequency (1.2 or 1.4 MHz). The attenuation coefficients were oil: 7.528 dB/m/MHz (Profound Medical Inc.), water: 0.22 dB/m/MHz [24], gel pad 5.791 dB/m/MHz (Profound Medical Inc.), fat: 60 dB/m/MHz [24], muscle: 57 dB/m/MHz [24], urine: 0.47 dB/m/MHz [25] and fibroid: 90 dB/m/MHz [26].

Delivered acoustic energy (E_A) was then calculated for each sonication using total attenuation (a_{total}) as follows:

$$E_A = P_A \cdot t \cdot 10^{\left(-\frac{a_{total}}{10}\right)} \quad (2)$$

where P_A is the acoustic power and t is the sonication time. Finally, volumes of 240 CEM43 contours and delivered acoustic energies at the focus were summed up over all sonications in order to determine heating efficiency (mL/J) for each fibroid.

2.6. Classification

Technical success of the treatment is usually measured by NPVr which is an objective and quantitative measure. Furthermore, the NPVr has been shown to correlate with the clinical treatment outcome [5,6]. Clinical success is commonly defined as at least a 10-point reduction in the symptom severity score (SSS) after the treatment [27]. An NPVr of more than 80% has been shown to result in clinical success in more than 80% of patients [6]. Correspondingly, the odds of clinical success have been shown to be 2.8 in those with an NPV of 30% or greater compared with those with an NPV of less than 30% [5]. Because of this rather robust correlation between the technical and clinical success as well as the objective nature of NPVr, the classification created in this study was based on NPVr rather than on SSS. The NPVr thresholds were chosen as

follows; an NPVr of more than 80% indicative of a good treatment outcome, an NPVr between 30% and 80% representing a moderate treatment outcome, and an NPVr less than 30% signifying a poor treatment outcome.

2.7. Statistical analysis

Statistical analysis was performed using JMP Pro statistical software version 13.1.0 (SAS Institute Inc.). A p -value less than 0.05 was considered statistically significant.

The normal distribution of each dataset was analyzed with the Shapiro–Wilk W test. Normally distributed numerical data are presented as mean \pm standard deviation and data with skewed distribution are presented as the median [interquartile range (IQR)]. The correlation between normally distributed parameters was analyzed by Pearson product-moment correlation and nonnormally distributed parameters were analyzed by Spearman's rank correlation analysis. Receiver-operating-characteristic (ROC) curve analyses were performed to determine optimal cutoff values. The whole models were examined using ROC curve analysis, and statistical significance was tested with the Chi-square test. Group means of normally distributed datasets were compared using Tukey–Kramer honestly significant difference (HSD) test for all pairs and nonnormally distributed datasets were compared using the Steel–Dwass method for all pairs.

3. Results

3.1. MRgHIFU treatment

Forty-two patients with forty-eight fibroids were treated without any significant adverse events. In all cases, nonperfused regions were detected after treatment, resulting in a median NPVr of 63.1% [40.3–82.7%]. An overview of the study population and MRgHIFU treatment parameters are shown in Table 2.

3.2. Diffusion-weighted imaging

The ADC maps were reconstructed with different combinations of b -values.

The median ADC value $1103 \times 10^{-6} \text{mm}^2/\text{s}$ [943–1188 $\times 10^{-6} \text{mm}^2/\text{s}$] with all b -values and $977 \times 10^{-6} \text{mm}^2/\text{s}$ [848–1055 $\times 10^{-6} \text{mm}^2/\text{s}$] with the highest b -values were similar.

Table 2. Summary of study population and MRgHIFU treatment parameters.

Characteristics	Value
Total number of patients	42
Total number of fibroids	48
Median age (years)	41 [37–43]
Median fibroid volume (mL)	72.1 [17.0–138.3]
Median total energy (kJ) per fibroid	112.7 [59.9–225.2]
Median total energy at the focus (kJ) per fibroid	28.8 [16.7–42.3]
Median total 240 CEM43 thermal dose volume (mL)	28.7 [6.5–60.3]
Median total treatment cell volume (mL)	28.9 [8.7–62.1]
Median NPV (mL)	25.2 [9.3–82.2]
Median NPV ratio (%)	63.1 [40.3–82.7]

NPV: nonperfused volume.

However, the mean ADC value of $2576 \pm 812 \times 10^{-6} \text{mm}^2/\text{s}$ with the lowest b-values was considerably higher.

3.3. Relationships between pretreatment MRI parameters and treatment efficiency parameters

Of the five pretreatment parameters, only ADC with the lowest b-values showed a significant correlation with heating efficiency (%) and only rT2(myoma/muscle) exhibited a significant correlation with the heating efficiency (mL/J). None of the pretreatment parameters correlated with the ablation efficiency. Four pretreatment parameters correlated significantly with the NPVr: ADC with all and the highest b-values, rT2(myoma/muscle) and rT2(myoma/myometrium). All *p*-values and Spearman's rank correlation coefficients (ρ) are shown in Table 3.

3.4. ADC and Funaki classifications

Based on the observed correlations only the ADC with all b-values was chosen for the classification analysis. The analysis

of the ROC curve indicated optimal ADC cutoff values of $980 \times 10^{-6} \text{mm}^2/\text{s}$ (NPVr > 80%) and $1800 \times 10^{-6} \text{mm}^2/\text{s}$ (NPVr < 30%), resulting in the following ADC classification: ADC I (NPVr > 80%), ADC II (NPVr 30–80%), and ADC III (NPVr < 30%). An example of pretreatment ADC maps, corresponding to the posttreatment T1-weighted contrast-enhanced images as well as screening T2-weighted images for each classification group are presented in Figure 2. Group means within the classifications were compared with all pairs Tukey–Kramer HSD test which revealed that there were no statistical differences between the Funaki classification group means, whereas there were statistically significant differences between the ADC classification group means (Figure 3). Over 30% of fibroids had a different ADC classification group than obtained from the Funaki classification (Figure 4). The means of fibroid volumes and treatment parameters displayed no statistically significant differences between the ADC or Funaki classification groups. A summary of the fibroid characteristics and MRgHIFU treatment parameters in each ADC and Funaki classification groups is presented in Table 4.

Table 3. Correlation coefficients (ρ) and *p*-values between pretreatment and treatment efficiency parameters.

Pretreatment parameter Statistical parameter	Heating efficiency (%)		Heating efficiency (mL/J)		Ablation efficiency (%)		NPVr (%)	
	ρ	<i>p</i> -Value	ρ	<i>p</i> -Value	ρ	<i>p</i> -Value	ρ	<i>p</i> -Value
ADC all b-values	−0.19	0.192	−0.18	0.216	−0.01	0.945	−0.31	0.034*
ADC lowest b-values	−0.32	0.029*	−0.05	0.734	−0.002	0.988	−0.23	0.119
ADC highest b-values	−0.27	0.064	−0.12	0.407	−0.08	0.580	−0.37	0.010*
rT2 (fibroid/muscle)	−0.25	0.083	−0.33	0.022*	−0.17	0.254	−0.34	0.020*
rT2 (fibroid/myometrium)	−0.18	0.221	−0.14	0.364	−0.20	0.180	−0.46	0.001*

*Statistically significant ($p < .05$); ADC: apparent diffusion coefficient; NPVr: nonperfused volume ratio; ρ : Spearman's rank correlation coefficient.

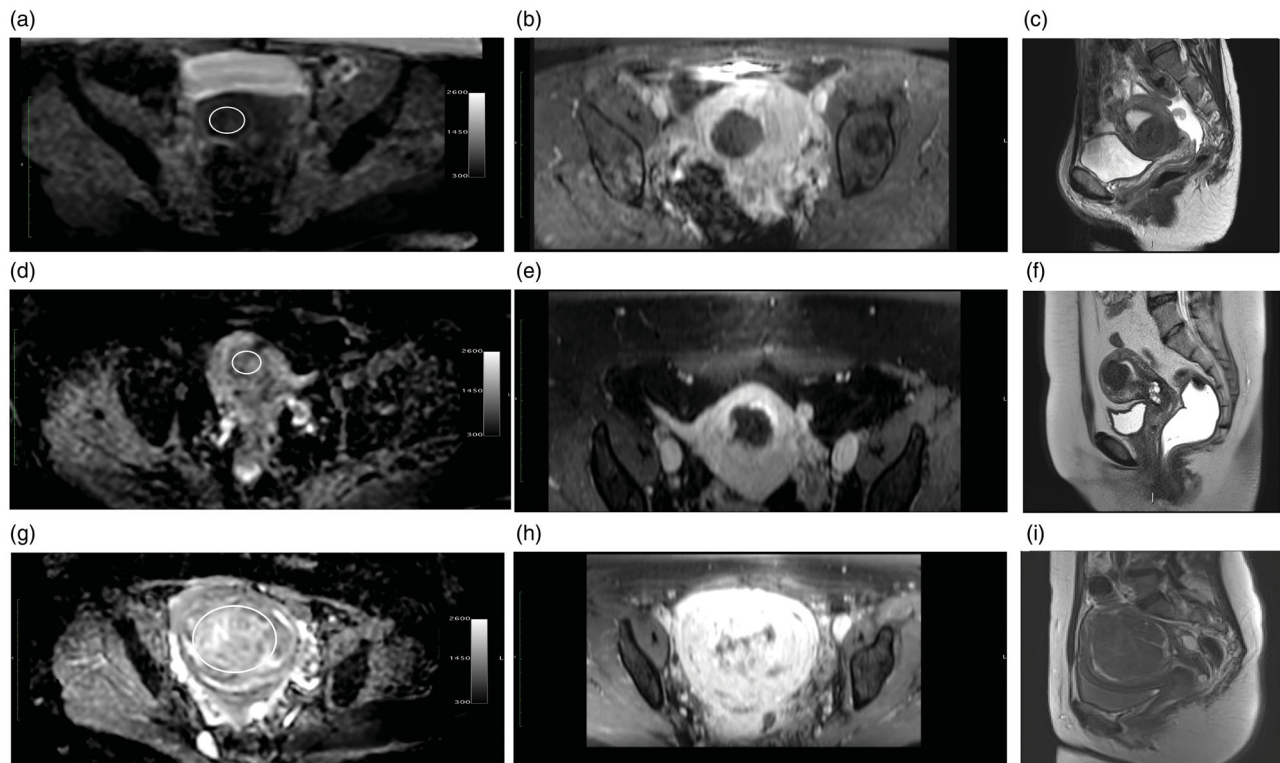


Figure 2. Example pretreatment axial ADC maps, corresponding posttreatment axial T1-weighted contrast-enhanced images illustrating the NPVr for each classification group, and screening MRI sagittal T2-weighted images illustrating Funaki classification: (a) ADC I: mean ADC value of $586 \times 10^{-6} \text{mm}^2/\text{s}$, (b) NPV ratio of 92%, and (c) Funaki II, (d) ADC II: mean ADC value of $1234 \times 10^{-6} \text{mm}^2/\text{s}$, (e) NPV ratio of 52%, and (f) Funaki I, and (g) ADC III mean ADC value of $2053 \times 10^{-6} \text{mm}^2/\text{s}$, (h) NPV ratio of 10% and (i) Funaki III.

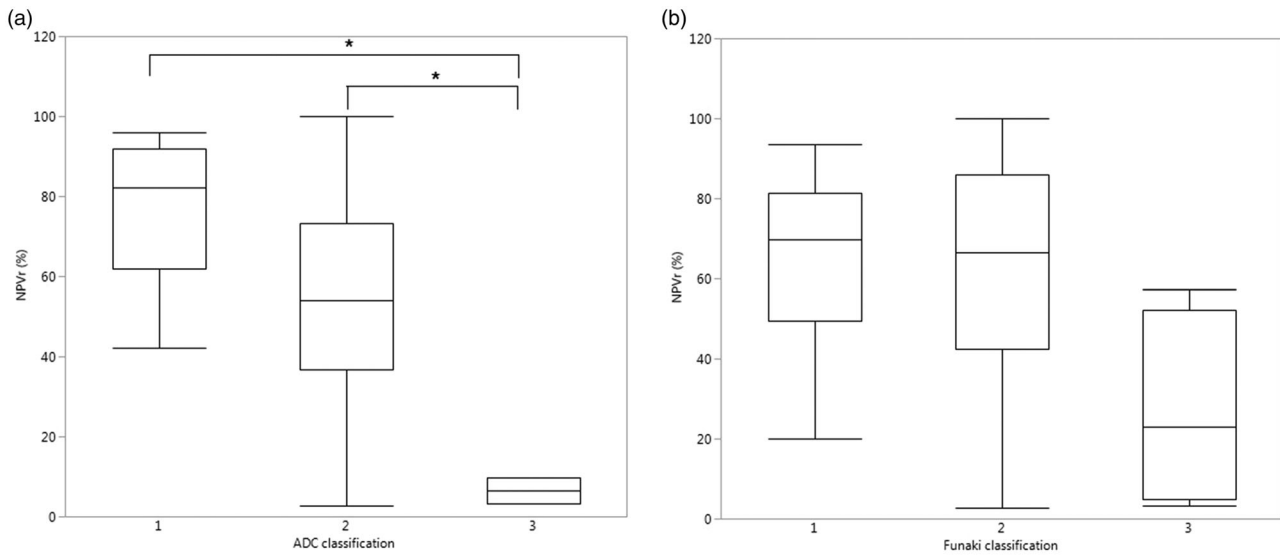


Figure 3. Box-Whisker plots presenting NPV ratios for (a) ADC classification and (b) Funaki classification groups, and group means within the classifications were compared with all pairs Tukey-Kramer HSD test. **p*-value < 0.05).

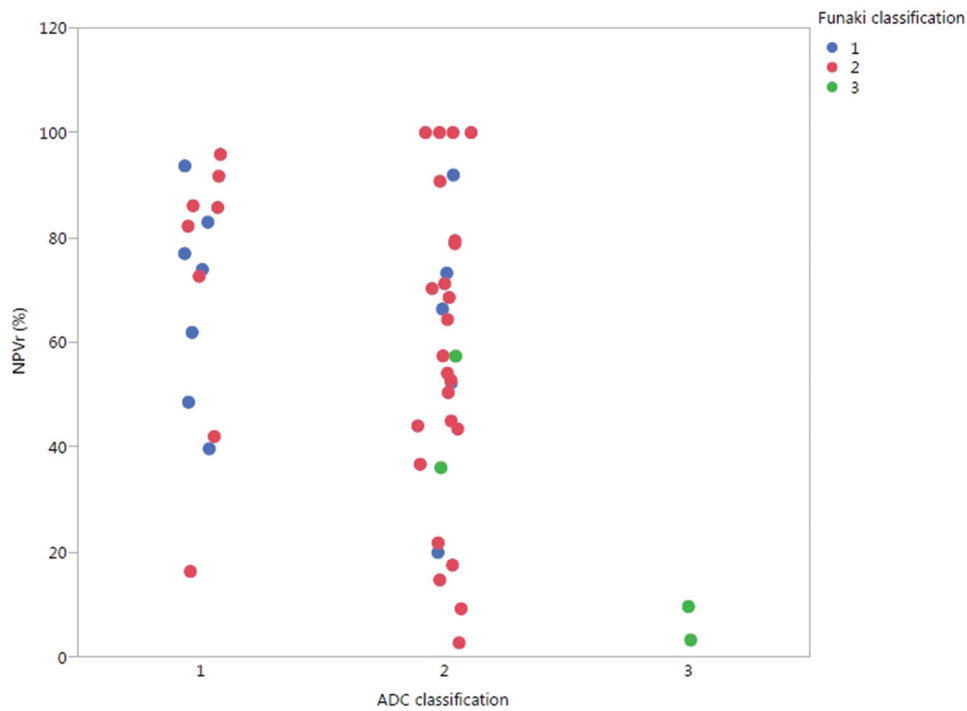


Figure 4. Scatter plot illustrating fibroids distribution between ADC and Funaki classification groups.

Table 4. Summary of fibroid characteristics and MRgHIFU treatment parameters in each ADC and Funaki classification group presented as median [interquartile range].

Parameter	ADC			Funaki		
	I	II	III	I	II	III
Total number of fibroids	15	31	2	12	32	4
Fibroid volume (mL)	24 [12–103]	89 [21–209]	168 [80–255]	75 [16–138]	62 [16–118]	135 [36–239]
Total energy (kJ)	94 [41–173]	124 [68–251]	263 [247–279]	115 [47–276]	112 [66–362]	224 [62–271]
Total energy at the focus (kJ)	22 [10–34]	27 [18–53]	39 [34–43]	22 [10–37]	28 [17–46]	39 [12–49]
Total 240 CEM43 thermal dose volume (mL)	20 [7–56]	33 [7–62]	8 [3–13]	27 [6–89]	32 [7–59]	9 [3–34]

ROC curve analysis by NPVr was performed for the ADC and Funaki classifications (Figure 5). The ADC classification resulted in the whole model area under the curve (AUC) value of 0.79 (*p*-value = 0.0007), whereas the AUC for the Funaki classification was 0.62 (*p*-value = 0.0527).

Linear regression analysis of the total volume of 240 CEM43 contours and the total delivered acoustic energy at the focus for each classification group showed statistically significant regression effect for ADC I, ADC II, Funaki I and Funaki II classification groups (Figure 6).

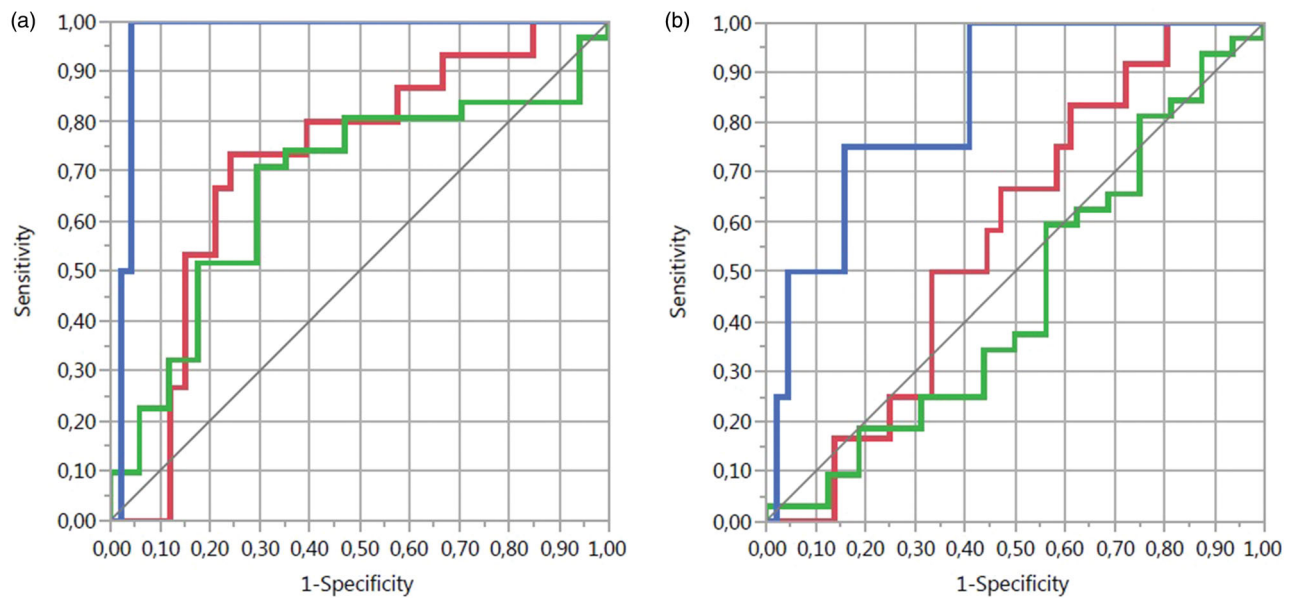


Figure 5. ROC curve analysis by NPVr was performed for (a) ADC classification and (b) Funaki classification, where area under curve values were for each classification group: ADC I 0.72, ADC II 0.67, ADC III 0.97, Funaki I 0.57, Funaki II 0.45, and Funaki III 0.84.

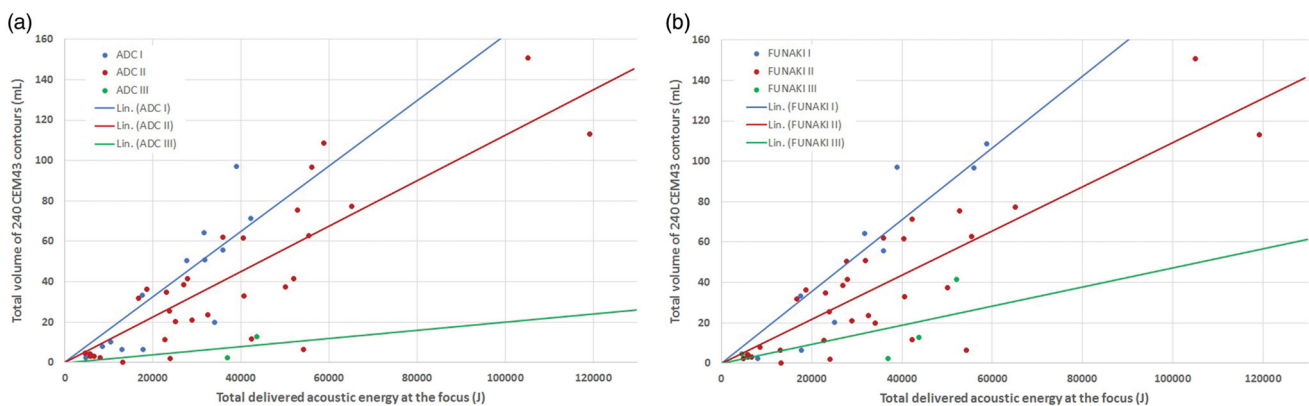


Figure 6. Linear regression analysis of the total volume of 240 CEM43 contours and the total delivered acoustic energy at the focus for a) ADC classification groups (ADC I: $R^2 = 0.71$ and p -value $< 0.0001^*$, ADC II: $R^2 = 0.71$ and p -value $< 0.0001^*$ and ADC III: $R^2 = 0.24$ and p -value = 0.32) and (b) Funaki classification groups (Funaki I: $R^2 = 0.85$ and p -value $< 0.0001^*$, Funaki II: $R^2 = 0.71$ and p -value $< 0.0001^*$ and Funaki III: $R^2 = 0.40$ and p -value = 0.08).

4. Discussion

T2-weighted SI of uterine fibroids and the Funaki classification are widely used predictors of the therapeutic efficacy of MRgHIFU treatment [2,10,28]. It has been recognized that fibroids with a high T2-weighted signal tend to display high cellularity relative to their fibrous content (i.e., increased water component), edema and/or degeneration, all of which predict poor tissue heating [7–9,29]. However, due to the relatively weak correlations and large overlap in NPV ratios between groups (also observed by Funaki et al. [10]), T2-based images may not be the optimal predictor of treatment outcome. High blood perfusion has also been shown to predict poor treatment efficacy, due to the rapid heat dissipation [11–14,30]. Quantitative dynamic contrast-enhanced MRI provides information about perfusion. However, the evaluation requires additional analysis and some expertise to obtain quantitative maps and is therefore not routinely used. Diffusion-weighted imaging (DWI) is a widely used MR imaging technique, and ADC post-processing can be done

automatically by the MRI scanner software making ADC information easily available for the radiologist. DWI can provide information about tissue structure, cellularity, and microcirculation [18], a previous study [31] indicated that DWI of uterine fibroids could provide information about both diffusion and perfusion effects, which are crucial determinants of the HIFU treatment outcome. Previous studies [11,13–15] with MRI parameters have revealed correlations with treatment efficiency parameters but they are difficult to apply in clinical use because there are no clear guidelines for the prediction of the treatment outcome by inspection of the treatment efficiency values. Classification with the NPVr could be a more informative as well as a more straightforward way to apply quantitative information into clinical use because NPVr correlates with clinical success [5,6].

The results of the current study indicate that median ADC value $1103 \times 10^{-6} \text{mm}^2/\text{s}$ [943 – $1188 \times 10^{-6} \text{mm}^2/\text{s}$] with all b-values was higher than median ADC value $977 \times 10^{-6} \text{mm}^2/\text{s}$ [848 – $1055 \times 10^{-6} \text{mm}^2/\text{s}$] with the highest b-values as expected. However, the difference was not statistically

significant. This might be due to the fact that the highest b-values used in this study do not emphasize diffusion effects sufficiently and, perhaps even higher b-values should have been used. The mean ADC value ($2576 \pm 812 \times 10^{-6} \text{mm}^2/\text{s}$) with the lowest b-values, on the other hand, were significantly higher than the other mean ADC values. These results suggest that there is a non-mono-exponential dependence between the signal decay and the b-value. This may support the hypothesis that DWI can reflect both diffusion and perfusion effects in uterine fibroids as described in a previous study [31].

T2-weighted signal ratios, ADC values obtained with all b-values, and ADC values acquired with only the highest b-values correlated with NPV ratios, which suggests that these could be good predictors of treatment outcomes. However, ADC values with the lowest b-values correlated only with heating efficiency (%). This can be attributable to the small sample size and the small number of lowest b-values. A greater number of lowest b-values could provide more accurate ADC values. This may warrant further investigations because ADC with the lowest b-values could provide perfusion information without the need for a contrast agent or the rather challenging analysis of quantitative dynamic contrast-enhanced imaging data. A new definition of heating efficiency (the total volume of 240 CEM43 contours divided by the total delivered acoustic energy at the focus) introduced in this study could hypothetically represent a more accurate definition for heating efficiency because it is not dependent on user-chosen treatment parameters or the anatomy of the patient. However, in our study, this parameter correlated only with $rT2(\text{fibroid}/\text{muscle})$. This is most likely due to this study's small sample size. Nevertheless, it may warrant further investigations due to the theoretically more accurate heating efficiency values compared to the currently used definition.

The ADC classification was divided into three groups: ADC I (NPVr > 80%), ADC II (NPVr 30–80%), and ADC III (NPVr < 30%) based on ROC curve analysis, which resulted in ADC cutoff values of $980 \times 10^{-6} \text{mm}^2/\text{s}$ and $1800 \times 10^{-6} \text{mm}^2/\text{s}$. The ROC curve analysis for the ADC-based classification and the T2-based classification [10] by NPV ratios showed that the ADC classification has higher sensitivity, specificity, and AUC values for each group. The classifications were then tested with the Chi-square test which revealed that only the ADC classification was a statistically significant predictor of the NPVr. This result supports our hypothesis that a quantitative method could be more reliable in predicting the treatment outcome.

Linear regression analysis of the total volume of 240 CEM43 contours and the total delivered acoustic energy at the focus for ADC and Funaki classification revealed statistically significant regression effect for ADC I, ADC II, Funaki I and Funaki II classification groups which may indicate that fibroids in different classification groups have different heating efficiencies (mL/J), for example, ADC I type fibroids have better heating efficiency than ADC II type fibroids. However, this warrants further investigations due to the small sample size in ADC III and Funaki III classification groups.

One of the limitations of this study is the small number of Funaki type III and ADC type III fibroids. This is mostly attributable to the fact that Funaki type III fibroids are usually excluded in the selection process and are not treated with MRgHIFU and the number of subjects could not be increased due to the use of oxytocin infusion during MRgHIFU treatment which has been shown to increase the treatment efficiency [32] and decrease the blood flow to the fibroid [33]. Oxytocin infusion during the treatment would therefore interfere with our interpretation of the results and patients treated after the completion of this study cannot be included any longer. Second, seventeen patients had their screening MRI performed with different MRI scanners with slightly different sequence parameters which may have affected the determination of the Funaki classification. Third, previous studies have shown that fibroid volume correlates with NPVr [6,34] which may be an additional factor affecting the ADC classification and the interpretation of the results. However, there were no statistically significant differences in median fibroid volumes between the classification groups which suggests that fibroid volume was not a significant factor in this study. Fourth, the total sample size was small, and the ADC classification could be further refined with a larger amount of data which would make it more sensitive and specific in predicting the NPVr. However, even with this small data set, the ADC classification was better in predicting the NPVr than its Funaki counterpart, suggesting that the ADC classification can be useful in patient selection for MRgHIFU treatment of uterine fibroids. Similar to our results, a recently published study indicated that a DWI based quantitative method could be more sensitive in discriminating different fibroid types than the Funaki classification prior to MRgHIFU therapy [35]. However, attention should be paid to diffusion-weighted imaging parameters when ADC value thresholds are used, because DWI sequence parameters, for example, repetition time, echo time, and choice of b-values can exert an impact on the calculated ADC values [36]. On the other hand, ADC values do not depend on the MR field strength under fixed imaging parameters [37–40].

In conclusion, lower ADC values correlate with higher NPV ratios. The ADC classification appears to be able to predict the NPV ratio prior to the MRgHIFU treatment and may even outperform the Funaki classification. The ADC classification could offer a novel, more reliable way of predicting the treatment outcome: ADC I for good treatment outcome ($\text{ADC} < 980 \times 10^{-6} \text{mm}^2/\text{s}$), and ADC II for moderate treatment outcome ($\text{ADC} 980\text{--}1800 \times 10^{-6} \text{mm}^2/\text{s}$), and ADC III for poor treatment outcome ($\text{ADC} > 1800 \times 10^{-6} \text{mm}^2/\text{s}$). Therefore, DWI with ADC maps should be included in the MRI screening protocol in the MRgHIFU treatment of uterine fibroids.

Acknowledgment

The authors acknowledge Saija Hurme, the biostatistician of Turku University, who kindly provided statistical advice in the preparation of this manuscript.

Disclosure statement

No potential conflict of interest was reported by the author(s).

Funding

This study has received funding from The Finnish Cultural Foundation, TYKS Foundation, and Instrumentarium Science Foundation.

ORCID

Teija Sainio  <http://orcid.org/0000-0001-5846-2601>
 Jani Saunavaara  <http://orcid.org/0000-0002-0617-1105>
 Gaber Komar  <http://orcid.org/0000-0001-5072-3782>
 Kirsi Joronen  <http://orcid.org/0000-0002-5527-8371>
 Antti Perheentupa  <http://orcid.org/0000-0002-1413-6414>
 Roberto Blanco Sequeiros  <http://orcid.org/0000-0002-0167-9639>

References

- [1] Stewart EA, et al. Sustained relief of leiomyoma symptoms by using focused ultrasound surgery. *Obstet Gynecol.* 2007;110:279–287.
- [2] Funaki K, Fukunishi H, Funaki T, et al. Mid-term outcome of magnetic resonance-guided focused ultrasound surgery for uterine myomas: from six to twelve months after volume reduction. *J Minim Invasive Gynecol.* 2007;14(5):616–621.
- [3] Funaki K, Fukunishi H, Sawada K. Clinical outcomes of magnetic resonance-guided focused ultrasound surgery for uterine myomas: 24-month follow-up. *Ultrasound Obstet Gynecol.* 2009;34(5):584–589.
- [4] Al Hilli M, Stewart E. Magnetic resonance-guided focused ultrasound surgery. *Semin Reprod Med.* 2010;28(3):242–249.
- [5] Fennessy FM, Tempany CM, McDannold NJ, et al. Uterine leiomyomas: MR imaging-guided focused ultrasound surgery—results of different treatment protocols 1. *Radiology.* 2007;243(3):885–893.
- [6] Mindjuk I, Trumm C, Herzog P, et al. MRI predictors of clinical success in MR-guided focused ultrasound (MRgFUS) treatments of uterine fibroids: results from a single centre. *Eur Radiol.* 2015;25(5):1317–1328.
- [7] Swe TT, et al. Uterine leiomyoma: correlation between signal intensity on magnetic resonance imaging and pathologic characteristics. *Radiat Med.* 1992;10:235–242.
- [8] Yamashita Y, Torashima M, Takahashi M, et al. Hyperintense uterine leiomyoma at T2-weighted MR imaging: differentiation with dynamic enhanced MR imaging and clinical implications. *Radiology.* 1993;189(3):721–725.
- [9] Oguchi O, Mori A, Kobayashi Y, et al. Prediction of histopathologic features and proliferative activity of uterine leiomyoma by magnetic resonance imaging prior to GnRH analogue therapy: correlation between T2-weighted images and effect of GnRH analogue. *J Obstet Gynaecol.* 1995;21(2):107–117.
- [10] Funaki K, et al. Magnetic resonance-guided focused ultrasound surgery for uterine fibroids: relationship between the therapeutic effects and signal intensity of preexisting T2-weighted magnetic resonance images. *Am J Obstet Gynecol.* 2007;196:1–6.
- [11] Kim Y-S, et al. Dynamic contrast-enhanced magnetic resonance imaging predicts immediate therapeutic response of magnetic resonance-guided high-intensity focused ultrasound ablation of symptomatic uterine fibroids. *Invest Radiol.* 2011;46:639–647.
- [12] Kim Y-s, Kim J-H, Rhim H, et al. High-intensity focused ultrasound ablation with a one-layer strategy to treat large uterine fibroids: initial clinical outcomes. *Radiology.* 2012;263(2):600–609.
- [13] Kim Y-s, Kim B-G, Rhim H, et al. Uterine fibroids: semiquantitative perfusion MR imaging parameters associated with the intraprocedural and immediate postprocedural treatment efficiencies of MR imaging-guided high-intensity focused ultrasound ablation. *Radiology.* 2014;273(2):462–471.
- [14] Wei C, et al. The predictive value of quantitative DCE metrics for immediate therapeutic response of high-intensity focused ultrasound ablation (HIFU) of symptomatic uterine fibroids. *Abdom Radiol.* 2017;43(8):2169–2175.
- [15] Hocquet A, Denis de Senneville B, Frulio N, et al. Magnetic resonance texture parameters are associated with ablation efficiency in MR-guided high-intensity focused ultrasound treatment of uterine fibroids. *Int J Hyperthermia.* 2017;33(2):142–149.
- [16] Kele PG, van der Jagt EJ. Diffusion weighted imaging in the liver. *World J Gastroenterol.* 2010;16(13):1567–1576.
- [17] Morani AC, Elsayes KM, Liu PS, et al. Abdominal applications of diffusion-weighted magnetic resonance imaging: where do we stand. *World J Radiol.* 2013;5(3):68–80.
- [18] Feuerlein S, Pauls S, Juchems MS, et al. Pitfalls in abdominal diffusion-weighted imaging: how predictive is restricted water diffusion for malignancy. *AJR Am J Roentgenol.* 2009;193(4):1070–1076.
- [19] Sainio T, Komar G, Saunavaara J, et al. Wedged gel pad for bowel manipulation during MR-guided high-intensity focused ultrasound therapy to treat uterine fibroids: a case report. *J Ther Ultrasound.* 2018;6:10.
- [20] Sapareto SA, Dewey WC. Thermal dose determination in cancer therapy. *Int J Radiat Oncol.* 1984;10(6):787–800.
- [21] Kim Y-s, Keserci B, Partanen A, et al. Volumetric MR-HIFU ablation of uterine fibroids: role of treatment cell size in the improvement of energy efficiency. *Eur J Radiol.* 2012;81(11):3652–3659.
- [22] Kim Y-s, Lee J-W, Choi CH, et al. Uterine fibroids: correlation of T2 signal intensity with semiquantitative perfusion MR parameters in patients screened for MR-guided high-intensity focused ultrasound ablation. *Radiology.* 2016;278(3):925–935.
- [23] Kim Y-s, Trillaud H, Rhim H, et al. MR thermometry analysis of sonication accuracy and safety margin of volumetric MR imaging-guided high-intensity focused ultrasound ablation of symptomatic uterine fibroids. *Radiology.* 2012;265(2):627–637.
- [24] Kyriakou A. Multi-physics computational modeling of focused ultrasound therapies [dissertation]. Komotini (Greece): Democritus University of Thrace; 2015.
- [25] Verma PK, Humphrey VF, Duck FA. Broadband measurements of the frequency dependence of attenuation coefficient and velocity in amniotic fluid, urine and human serum albumin solutions. *Ultrasound Med Biol.* 2005;31(10):1375–1381.
- [26] Keshavarzi A, Vaezy S, Kaczkowski PJ, et al. Attenuation coefficient and sound speed in human myometrium and uterine fibroid tumors. *J Ultrasound Med.* 2001;20(5):473–480.
- [27] Stewart EA, Rabinovici J, Tempany CMC, et al. Clinical outcomes of focused ultrasound surgery for the treatment of uterine fibroids. *Fertil Steril.* 2006;85(1):22–29.
- [28] Lénárd ZM, McDannold NJ, Fennessy FM, et al. Uterine leiomyomas: MR imaging-guided focused ultrasound surgery-imaging predictors of success. *Radiology.* 2008;249(1):187–194.
- [29] Ueda H, Togashi K, Konishi I, et al. Unusual appearances of uterine leiomyomas: MR imaging findings and their histopathologic backgrounds. *Radio Graph.* 1999;19(1):S131–S145.
- [30] Wang Y, Ren D, Wang W. The influence of oxytocin on the blood perfusion of uterine fibroids: contrast-enhanced ultrasonography evaluation. *J Med Ultrasound.* 2016;24(1):13–17.
- [31] Ikink ME, Voogt MJ, van den Bosch MAAJ, et al. Diffusion-weighted magnetic resonance imaging using different b-value combinations for the evaluation of treatment results after volumetric MR-guided high-intensity focused ultrasound ablation of uterine fibroids. *Eur Radiol.* 2014;24(9):2118–2127.
- [32] Lozinski T, Filipowska J, Krol P, et al. Oxytocin administration in high-intensity focused ultrasound treatment of myomata. *Biomed Res Int.* 2018;2018:7518026.
- [33] Otonkoski S, Sainio T, Komar G, et al. Oxytocin selectively reduces blood flow in uterine fibroids without an effect on myometrial

- blood flow: a dynamic contrast enhanced MRI evaluation. *Int J Hyperthermia*. 2020;37(1):1293–1300.
- [34] Suomi V, et al. Comprehensive feature selection for classifying the treatment outcome of high-intensity ultrasound therapy in uterine fibroids. *Sci Rep*. 2019;9:1–11.
- [35] Andrews S, Yuan Q, Bailey A, et al. Multiparametric MRI characterization of Funaki types of uterine fibroids considered for MR-guided high-intensity focused ultrasound (MR-HIFU) therapy. *Acad Radiol*. 2019;26(4):e9–e17.
- [36] Celik A. Effect of imaging parameters on the accuracy of apparent diffusion coefficient and optimization strategies. *Diagn Interv Radiol*. 2016;22(1):101–107.
- [37] Donati OF, Chong D, Nanz D, et al. Diffusion-weighted MR imaging of upper abdominal organs: field strength and intervendor variability of apparent diffusion coefficients. *Radiology*. 2014;270(2):454–463.
- [38] Ogura A, et al. Apparent diffusion coefficient value is not dependent on magnetic resonance systems and field strength under fixed imaging parameters in brain. *J Comput Assist Tomogr*. 2015;39:760–765.
- [39] Eghedari M, Ma J, Fox P, et al. Effects of magnetic field strength and b value on the sensitivity and specificity of quantitative breast diffusion-weighted MRI. *Quant Imaging Med Surg*. 2016;6(4):374–380.
- [40] Merhemic Z, Imsirovic B, Bilalovic N, et al. Apparent diffusion coefficient reproducibility in brain tumors measured on 1.5 and 3 T clinical scanners: a pilot study. *Eur J Radiol*. 2018;108:249–253.